Float Observations of the Southern Ocean. Part II: Eddy Fluxes

SARAH T. GILLE

Scripps Institution of Oceanography, and Department of Mechanical and Aerospace Engineering, University of California, San Diego, La Jolla, California

ABSTRACT

Autonomous Lagrangian Circulation Explorer (ALACE) floats are used to examine eddy fluxes in the Southern Ocean. Eddy fluxes are calculated from differences between ALACE float data and mean fields derived from hydrographic atlas data or objectively mapped float observations. Heat fluxes indicate an average poleward eddy heat transport across the Antarctic Circumpolar Current (ACC) of about 3–7 kW m^{-2} at 900-m depth. Because analysis of current meter data suggests that ALACE's 9–25-day averaging underestimates the total heat flux, the initial ALACE estimates are rescaled to account for this undersampling. This results in a total corrected heat flux of 5–10 kW m^{-2} at 900 m, depending on the mean field used for the calculations. If the cross-ACC heat flux is assumed to vary exponentially through the water column with an e-folding depth of 1000 m, then the implied net poleward heat flux across the ACC is between 0.3 ± 0.1 and 0.6 ± 0.3 ($\times 10^{15}$ W). These estimates are in agreement with previous Southern Ocean eddy flux estimates, which have suggested a cross-ACC heat fluxes ranging between 0.05 and 0.9 ($\times 10^{15}$ W). Cross-stream fluxes vary geographically, with the largest fluxes occuring in the Indian Ocean sector, near the Agulhas Retroflection. Statistically significant poleward fluxes also occur along the core of the ACC. Along-stream fluxes are comparable in size to cross-stream fluxes. Momentum fluxes observed by ALACE are isotropic and do not indicate statistically significant eddy–mean flow interactions.

1. Introduction

Poleward heat fluxes in the ocean roughly equal poleward heat fluxes in the atmosphere (Keith 1995; Bryden and Imawaki 2001). In closed ocean basins, western boundary currents provide a pathway to transport heat meridionally, but the Southern Ocean contains no continental boundaries, and the quasi-zonal Antarctic Circumpolar Current (ACC) acts as a barrier to poleward heat transport. Because there is no pathway for mean heat transport across the ACC, eddies are thought to be responsible for poleward heat transport across the Southern Ocean (deSzoeke and Levine 1981). This paper takes advantage of Autonomous Lagrangian Circulation Explorer (ALACE) float observations to look at the Southern Ocean eddy heat and momentum fluxes that link the subtropical gyres of the Pacific, Atlantic, and Indian Oceans with the ACC.

Because of the thermal wind effect, isopycnal surfaces at the core of the ACC tilt strongly upward to the south, and most isopycnals outcrop within the ACC. Since water parcels preferentially mix along isopycnals rather than across them, mixing is expected to bring deep water into contact with the atmosphere, rather than carrying heat poleward toward the Antarctic coast. The

ACC thus is hypothesized to be a barrier to horizontal mixing, and cross-ACC heat transport is expected to depend on diapycnal processes. Table 1 summarizes previous estimates of cross-ACC eddy heat fluxes. Estimates of oceanic heat loss to the atmosphere, suggest that the ocean should transport 0.3×10^{15} W poleward across the ACC (Gordon and Owens 1987). Other estimates summarized in Table 1 range from 0.05 to 0.9 $\times 10^{15}$ W, depending on the locations of the measurements and the methodology. On the basis of their analysis of hydrographic data, deSzoeke and Levine (1981) estimated low meridional overturning and conjectured that eddy processes should be responsible for all of the poleward heat flux.

Despite the hypothesized importance of eddy processes in the Southern Ocean heat budget, no direct measurements of the cross-ACC eddy transport have been available on a global scale. Estimates of eddy heat fluxes across the ACC require repeated measurements of both temperature and velocity. While current meters provide point estimates of heat fluxes, coverage has been sparse (e.g., Wunsch 1999), and there has been no means to determine whether these isolated measurements are reliable indicators of zonally integrated meridional heat fluxes.

Recent inverse models incorporating Southern Ocean hydrographic data (Macdonald and Wunsch 1996; Gille 1999; Sloyan and Rintoul 2000; Ganachaud and Wunsch

Corresponding author address: Dr. Sarah T. Gille, Scripps Institution of Oceanography, San Diego, La Jolla, CA 92093-0230.
E-mail: sgille@ucsd.edu

TABLE 1. Selected estimates of cross-ACC eddy heat flux. Negative values reported here reflect poleward eddy heat flux across the identified location.

Reference	Location	Local flux (kW m²)	Integrated transport (10¹⁵W = PW)
	Current meters		
Bryden (1979)[a]	Drake Passage (2700 m)	−6.7	−0.5
Sciremammano et al. (1980)	Drake Passage (1000–2500 m)	−17	
Nowlin et al. (1985)	Drake Passage (500–2700 m)	−3.7[b]	
Johnson and Bryden (1989)	Drake Passage (580–3560 m)	−12	
Phillips and Rintoul (2000)	51°S, 143°E (400–3300 m)	−11.3[b], −40.6[c]	
	Hydrography		
deSzoeke and Levine (1981)	ACC		−0.45
Macdonald and Wunsch (1996)	30°S		−0.9 ± 0.3
Sloyan and Rintoul (2000)	30–40°S		−0.36 ± 0.08
Ganachaud and Wunsch (2000)	20–30°S		−0.7 ± 0.3
	Altimetry		
Keffer and Holloway (1988)	ACC (∼53°S)		−0.70
Stammer (1998)	40°S		−0.3
	53°S		−0.05
	Global energy balance		
Gordon and Owens (1987)	ACC		−0.31

[a] See Nowlin et al. (1985) for results reported in mks units.
[b] Bandpass filtered in time.
[c] All frequencies.

2000) provide estimates of the net meridional heat transport, but hydrographic coverage of the Southern Ocean is limited. Since measurements have not been repeated along zonal lines in the Southern Ocean, inverse models cannot distinguish meridional eddy fluxes from mean heat fluxes. Studies based on hydrographic data have indicated that heat enters the Southern Ocean within the Indian Ocean sector and exits in the Pacific and Atlantic sectors (Georgi and Toole 1982; Macdonald and Wunsch 1996; Sloyan and Rintoul 2000; Ganachaud and Wunsch 2000); much of the heat that enters in the Indian Ocean, however, appears to recirculate through the Indonesian Throughflow (J. M. Toole 2000, personal communication).

Heat fluxes are expected to show substantial geographic variability that will not be well sampled by isolated current meters or basin-scale inverse models. Satellite altimeter data indicate that eddy activity varies significantly along the path of the ACC. In eddy heat flux estimates based on altimeter measurements, regions of high eddy kinetic energy and high meridional temperature gradients are conjectured to be regions of high eddy heat fluxes (Keffer and Holloway 1988; Stammer 1998). However, these estimates rely on an assumption that eddy heat fluxes are proportional to large-scale temperature gradients, and they therefore do not allow for the possibility of equatorward heat transport nor do they probe below the ocean's surface.

Although heat transport is expected to occur predominantly along isopycnals, fluxes computed from current meters, surface observations, or isobaric floats represent mixing at constant depth. These isobaric fluxes can be projected into along-isopycnal and diapycnal components. Where isopycnals are flat, the isobaric fluxes will be equivalent to along-isopycnal fluxes. If isopycnals rose vertically, then isobaric fluxes would represent diapycnal processes. Since along-isopycnal mixing is expected to be large compared with diapycnal mixing, one might imagine that isobaric fluxes should be slightly smaller in the core of the ACC, where isopycnals are strongly tilted.

In this study, ALACE displacement data are used in combination with the mean fields that are discussed in a companion paper (Gille 2003, henceforth Part I), to estimate isobaric Southern Ocean heat and momentum fluxes at middepth. The methodology used here allows heat fluxes to be estimated throughout the Southern Ocean, in contrast with heat flux estimates from isolated current meters or single hydrographic sections which can represent only a limited geographic region. Section 2 discusses the method used to compute eddy heat and momentum fluxes. Section 3 evaluates the degree to which ALACE floats are likely to undersample true fluxes by examining existing current meter observations from the Southern Ocean. Corrected results are discussed in section 4. Spatial variations of heat fluxes can be assessed, and these variations are used to evaluate whether the sloping isopycnals of the ACC actually do inhibit meridional heat flux. The findings are summarized in section 5.

2. Method: Eddy fluxes from ALACE

a. Method: Defining fluxes

ALACE floats provide quasi-Lagrangian measurements of temperature and velocity, averaged over 9–25-

day intervals. Details of Southern Ocean ALACE temperature and velocity measurements are reviewed in Part I. The floats are ballasted to a predetermined depth, so their motions are predominantly along constant depth surfaces rather than isopycnals. Southern Ocean ALACE measurements have an average pressure near 900 dbar, and this study will focus on the fields at 900 m.

Analyses of Lagrangian float data often employ dispersion statistics determined from the long-term evolution of extended float trajectories. However, ALACE floats are not suited for this kind of analysis, because they spend 24 hours on the ocean surface at the end of each measurement cycle, where they behave like undrogued drifters that are blown by the wind (Gille and Romero 2003). In addition, ALACEs do not resolve temperature or velocity fluctuations on timescales shorter than a measurement cycle but return only the time-averaged temperature and total position displacement for the duration of the cycle. Interpreting eddy statistics from the data therefore requires an alternate approach. In this paper, each ALACE displacement is treated much like a single Eulerian measurement from a current meter located at the center point of the ALACE trajectory.

At any given point in time, the ACC can be thought of as a series of narrow jets of about 100-km width, characterized by rapid temperature change, as depicted by the dashed lines in Fig. 1. Over time, each jet meanders meridionally with a range of about 100 km so that the instantaneous jet position shifts. In Fig. 1, the dashed lines indicate the positions of the jet at three separate points in time, and the time mean is represented by the solid line. A current meter placed at fixed depth in the middle of the mean jet (the gray line at 0 km in Fig. 1a) will measure the downstream flow of the jet, the cross-stream velocities due to the meandering of the jet, and temperature anomalies resulting from the difference between the time averaged and instantaneous temperatures. For comparison, floats deployed in the jet will be advected downstream and will also move meridionally with the meandering fronts. Figure 1b indicates the temperature that might be recorded by three independent floats deployed at different points in time and at different locations relative to the mean axis of the current. During each measurement cycle, we expect that a typical float will migrate cross stream with the front, maintaining a roughly constant temperature. Thus a single float observation will not provide information about the time-averaged temperature or velocity at a given location, but the combined data from many independent floats will allow us to estimate the mean temperature and velocity over a broad geographic region spanning the full length and width of the current. Note that the approach used here differs substantially from the framework described by Bower (1991) or by Lozier et al. (1996) who examined cross-stream fluxes relative to a coordinate frame that moved with the meandering
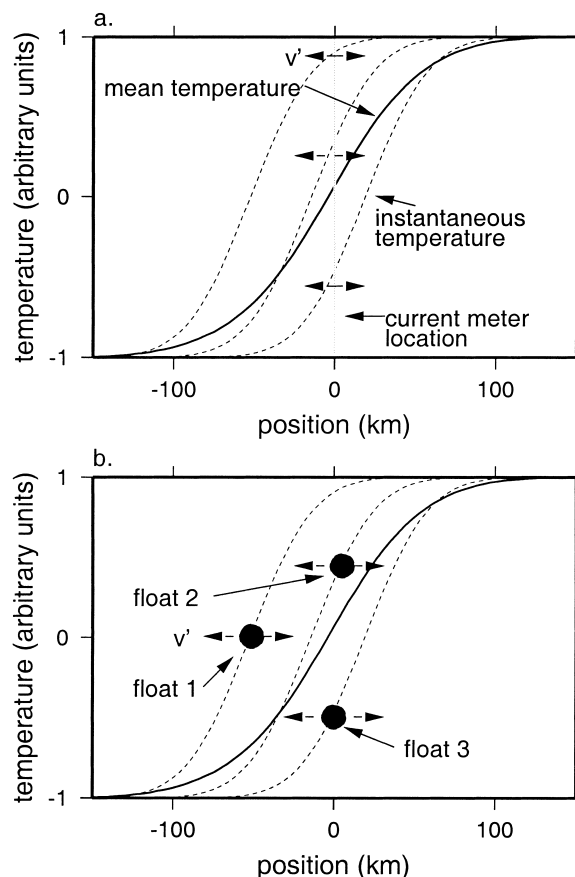

FIG. 1. Schematic illustrating mean cross-stream temperature at a fixed depth across one of the frontal features that compose the ACC (solid line) and instantaneous temperatures across the front at three separate points in time (dashed lines). (a) A current meter located at the center of the stream will observe temperature changes and meridional velocities associated with the northward and southward migrations of the front. (b) Floats deployed at different locations across the front will migrate with the front measuring the meridional velocity associated with the meandering. During each sampling cycle, individual floats may remain on fixed temperature contours, so they do not observe temperature fluctuations. Geographically distributed, independent float observations can be combined to determine a mean, however, so that instantaneous temperatures at an observation location can be compared with time-averaged temperatures at the same location.

current. This analysis is strictly concerned with motions relative to the time-mean flow.

This study estimates heat and momentum fluxes by computing differences between individual ALACE measurements and mean fields. Figure 2 illustrates the method schematically. Temperature and velocity measurements from each "instantaneous" ALACE displacement are compared with mapped mean temperature and velocities that have been interpolated onto the locations of the ALACE measurements. The mapped time-mean streamlines are used to project the total ALACE velocity **u** (solid arrow in Fig. 2) into orthogonal components, u and v (dashed arrows), in the along-stream and cross-stream components, respectively. At the same location,
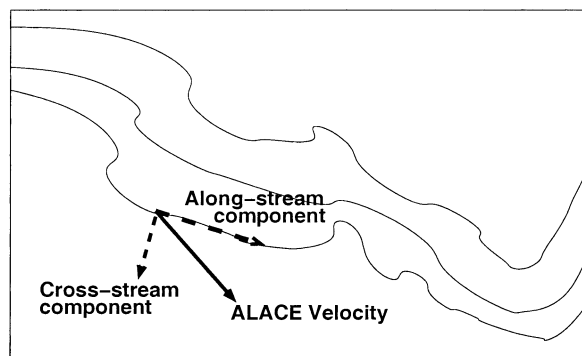
FIG. 2. Schematic illustrating projection of instantaneous ALACE velocity (solid vector) into along-stream and cross-stream components (dashed vectors) relative to the time-mean streamlines (thin lines).

the time-mean velocity $\overline{u}$ is also calculated from dynamic height contours to represent the mean circumpolar flow. The along-stream anomaly u' is $u - \overline{u}$, and the cross-stream velocity anomaly v' is equivalent to v since $\overline{v}$ is defined to be zero. The potential temperature anomaly $\theta' = \theta - \overline{\theta}$ is determined from the difference between ALACE and time-mean estimates. Eddy heat transports $(\rho C_p \langle \mathbf{u}' \theta' \rangle)$ and momentum transports (e.g., $\langle u'v' \rangle$) are then computed, where ρ is density and is taken to be 1035 kg m^{-3}, and C_p is the specific heat of water at constant pressure and is taken to be 4000 J kg^{-1} °C^{-1}.

Here overbars specifically denote time means at a single location, while angle brackets denote averages that can be spatial as well as temporal. Primes are anomalies relative to the local time mean. By definition, the means of $\overline{u'}$ and $\overline{\theta'}$ are zero. Using standard Reynolds averaging, we expect that formally $\overline{\mathbf{u}' \theta'} = \overline{(\mathbf{u} - \overline{\mathbf{u}})\theta} = \overline{\mathbf{u}(\theta - \overline{\theta})}$. Therefore, if perfect data were available, it would be possible to estimate the eddy flux quantities by knowing the time-averaged value of either θ or $\mathbf{u}$. In reality the data coverage is variable, and we work with spatiotemporal averages that do not necessarily have zero mean. Thus this study relies on separate estimates of $\overline{\mathbf{u}}$ and $\overline{\theta}$, as discussed in the companion paper, Part I.

The presence of a meandering jet, as depicted in Fig. 1, will not automatically result in poleward eddy heat flux. For example, if the instantaneous temperature structure in Fig. 1 is always the same, then northward and southward motions will cancel each other out, and $\overline{v'\theta'}$ will be zero. (This is true regardless of whether floats or current meters are used.) In order to have a net heat flux, the average temperature of northward-moving water must differ from that of southward-moving water. These temperature differences can be caused by mixing associated with particle motions within a jet (e.g., Owens 1984; Bower 1991; Lozier et al. 1996) and by the formations of rings and eddies associated with baroclinic instability of the flow. Since float temperatures

and velocities are 9–25-day averages, high-frequency components of the eddy flux cannot be determined from floats, and the details of these physical processes cannot readily be explored using ALACE data. Thus the analysis in this paper is focused on bulk eddy flux estimates rather than specific processes.

b. Estimated fluxes

Eddy heat and momentum fluxes estimated from ALACE data are presented in Table 2. Here means are derived either from the objectively mapped fields computed directly from the ALACE data, as presented in Part I, or from gridded hydrographic data produced by Gouretski and Jancke (1998, henceforth GJ). Case A uses a mean based on ALACE observations, mapped using an isotropic Gaussian covariance function with a decorrelation scale of 495 km, a signal-to-noise ratio of 2, and initial-guess fields for the dynamic topography based on atlas data referenced to 3500-m depth. As indicated in Part I, gridded fields are sensitive to the parameters used to map, so a variety of other mean fields are explored. Cases B through F are like case A except that they use differing decorrelation scales. Cases G and H resemble case A except that the signal-to-noise ratios are changed to 1 and 4, respectively. Case I assumes that the temperature and dynamic height fields decorrelate more slowly along streamlines than across them. Cases J and K are like case A but use initial-guess dynamic topography fields referenced to 3000 and 4000 m, respectively. Case M is an optimal combination of case A and atlas data. The final three cases are based solely on GJ's hydrography at 900-m depth, with dynamic topography referenced to 3000, 3500, or 4000 m. The parameters defining these cases are presented in detail in Table 1 of Part I. This wide range of definitions of means is used because eddy flux estimates are sensitive to the choice of mean. The discussion of resulting fluxes will focus on signals that are not strongly dependent on the choice of mean.

For ease in comparing the subsurface heat fluxes with fluxes computed in other studies at a variety of depths, heat fluxes are computed based on potential temperature referenced to the surface. Since salinity measurements are not uniformly available, a constant salinity of 34 psu is assumed in the potential temperature calculations. In practice the difference between fluxes computed from temperature and fluxes computed from potential temperature is negligible.

ALACE measurements are used for this analysis if they come from regions with time-averaged dynamic heights in a range corresponding to the core of the ACC, as described in the caption to Table 2. This dynamic height range was chosen in order to focus this analysis on the portion of the Southern Ocean that is best sampled by float data and to minimize the impact of the subtropical gyres and Agulhas Retroflection, which differ dynamically from the ACC. Within statistical error

TABLE 2. Averaged eddy heat and momentum fluxes at 900-m depth in the Southern Ocean determined from ALACE float anomalies relative to objectively mapped fields from atlas data and from ALACE data. The dynamic height range used to delineate the ACC core was from 0.62 to 1.12 m for dynamic heights referenced to 3000 m, from 0.8 to 1.3 m for dynamic heights referenced to 3500 m (equivalent to -0.25 to 0.25 m in Figs. 2c,d in Part I), and from 0.95 to 1.35 m for dynamic heights referenced to 4000 m. Here velocity components have been rotated into stream coordinates so that u' is the velocity anomaly in the along-stream direction and v' is the velocity anomaly in the cross-stream direction. Temperatures are converted to potential temperatures assuming a uniform salinity of 34 psu. Error bars represent the standard error about the mean and are equivalent to one standard deviation divided by the square root of the number of independent observations. Parameters defining cases A–M are defined in Table 1 in Part I.

Case	Heat flux (kW m^{-2})		Momentum flux (cm^2 s^{-2})		
	$\rho C_p \langle u'\theta' \rangle$	$\rho C_p \langle v'\theta' \rangle$	$\langle u'u' \rangle$	$\langle v'v' \rangle$	$\langle u'v' \rangle$
	Mean fields from floats				
A	1.2 ± 3.0	-4.9 ± 1.4	55 ± 8	44 ± 7	1.8 ± 1.4
B	2.2 ± 2.6	-3.2 ± 1.8	57 ± 7	45 ± 6	0.1 ± 1.3
C	2.9 ± 2.9	-4.5 ± 2.8	66 ± 8	45 ± 6	1.1 ± 1.1
D	0.6 ± 1.9	-5.6 ± 1.5	49 ± 8	43 ± 7	2.6 ± 1.2
E	0.5 ± 1.9	-5.8 ± 1.6	52 ± 8	42 ± 7	2.8 ± 1.4
F	-0.8 ± 1.5	-5.8 ± 1.3	45 ± 8	41 ± 8	2.9 ± 1.3
G	1.2 ± 2.9	-5.7 ± 1.3	56 ± 8	46 ± 7	1.6 ± 1.2
H	1.6 ± 2.6	-4.7 ± 1.4	53 ± 8	44 ± 6	2.0 ± 1.1
I	0.2 ± 4.3	-4.3 ± 1.5	69 ± 10	47 ± 6	1.6 ± 1.3
J	0.8 ± 2.4	-5.1 ± 1.4	54 ± 8	44 ± 6	1.5 ± 1.1
K	0.9 ± 2.8	-5.2 ± 1.5	56 ± 9	45 ± 7	2.0 ± 1.2
	Mean fields from merged atlas and float				
M	8.5 ± 2.6	-5.1 ± 1.4	59 ± 10	48 ± 9	0.7 ± 1.0
D_{ref} (m)	Mean fields from atlas				
3000	17.8 ± 6.0	-4.8 ± 4.5	64 ± 10	49 ± 8	-1.1 ± 1.4
3500	21.2 ± 6.4	-5.8 ± 3.9	63 ± 10	46 ± 8	-1.1 ± 1.4
4000	14.5 ± 6.0	-6.7 ± 4.6	64 ± 10	49 ± 8	-1.0 ± 1.4

bars, cross-stream eddy fluxes ($\rho C_p \langle v'\theta' \rangle$ as well as $\langle v'v' \rangle$) for the full dataset are the same as the ACC core eddy fluxes reported here. Regardless of the choice of mean fields, this analysis implies that the meridional eddy heat transport across the ACC is poleward and between 3.2 and 6.7 kW m^{-2}.

Error bars represent the standard error about the mean and are equivalent to one standard deviation divided by the square root of the number of observations. Statistical error bars range between 1.3 and 2.8 kW m^{-2} for cases using float data as a mean. Estimates based on atlas means have larger errors. This occurs because the atlas means differ substantially from the float means in some locations such as the Agulhas Retroflection region, and as a result the eddy fluxes have larger variances.

Part I reports that float temperatures are systematically warmer than atlas temperatures, implying a long-term warming trend in the Southern Ocean. This temperature bias suggests that fluxes based on the atlas mean will appear larger than fluxes based on the float mean. However, because results based on atlas data have large statistical errors, the differences between atlas and float means are not discernibly different within error bars.

In contrast with the cross-stream fluxes, eddy fluxes that depend on the along-stream anomaly u' depend strongly on the choice of mean. Along-stream eddy heat fluxes range from -0.8 to 21.2 kW m^{-2}; fluxes based on float-derived means do not differ from zero within error bars, while fluxes based on atlas means are some-

what larger. This difference occurs because $\overline{u}$ is smaller in the atlas fields than in the ALACE-derived fields as discussed in Part I. Long-term temperature trends do not appear to have a strong influence on the difference. Along-stream eddy fluxes outside the core ACC (not shown here) tend to be smaller or more negative than the fluxes in Table 2 because the statistics of the along-stream mean are different inside and outside the jet core.

Mean heat transports are not reported in Table 2 since they depend on the arbitrary scale used to measure temperature; in general they are an order of magnitude or more larger than the eddy heat fluxes. The $\langle u'u' \rangle$ and $\langle v'v' \rangle$ momentum fluxes are comparable to each other in magnitude with values between 40 and 70 cm^2 s^{-2}. The covariance terms $\langle u'v' \rangle$ are positive for ALACE means and negative for atlas means, but they are an order of magnitude smaller than the other terms and are not consistently statistically different from zero.

ALACE data coverage is more extensive in the highly energetic Atlantic sector of the Southern Ocean than in the eastern Indian or Pacific Oceans. There is, however, little evidence for a distortion in the eddy heat flux estimates as a result of this geographic bias. Within statistical error bars, eddy heat fluxes based on float means for the region between 60°E and 60°W spanning the Indian and Pacific Oceans are generally equivalent to the fluxes reported here. Eddy heat fluxes based on atlas means in the Indo–Pacific subregion are equatorward on average but have large error bars, so this difference may not be significant. Eddy momentum fluxes
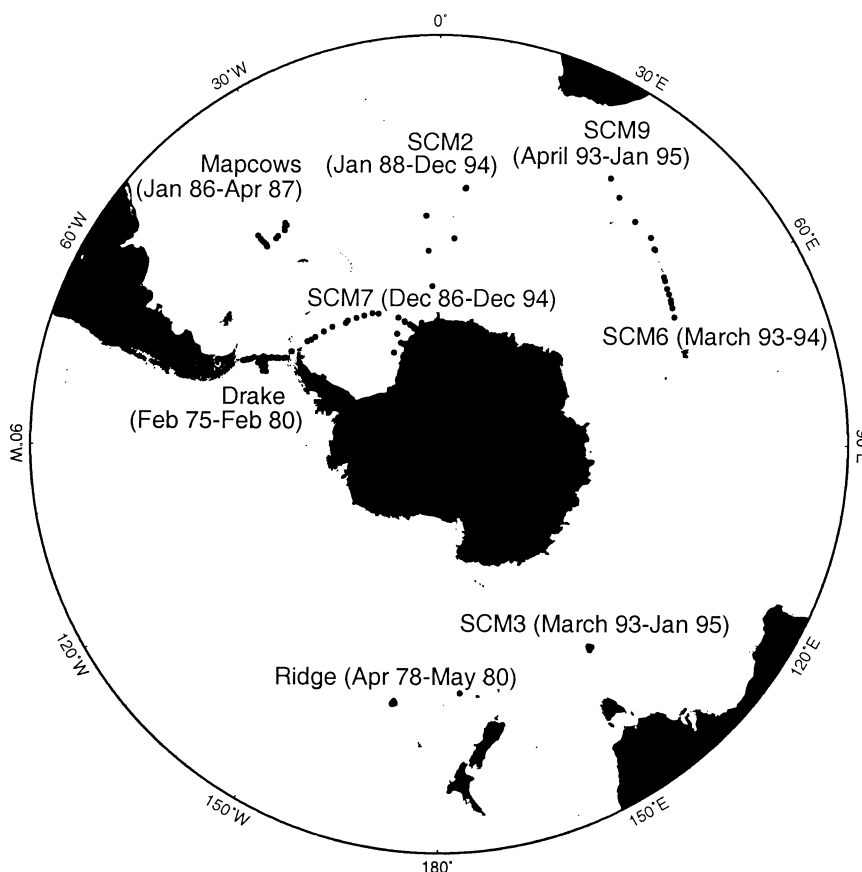
FIG. 3. Locations of 339 current meters available for this study (online at kepler.oce.orst.edu/cmdac.html). Dates indicate starting and ending dates for current meters in field region. Redeployments were treated as separate records in this analysis. Depths ranged from 30 to 5900 m.

in the Indo–Pacific subregion are slightly less energetic than eddy momentum fluxes in Table 2; this occurs in part because the flow is less well sampled, and so the instantaneous velocities may not be as well differentiated from the mean flow.

3. The missing high-frequency component: Fluxes from current meters

Evaluations of numerical model output and in situ measurements have shown that the Southern Ocean experiences substantial high-frequency variability (e.g., Fukumori et al. 1998; Gille and Hughes 2001) that will be smoothed by ALACE sampling. In an analysis of Drake Passage current meter records Nowlin et al. (1985) estimated that most of the poleward eddy heat flux was contained in the 6–90-day time band, with about one-half of this energy at time periods less than 35 days. Similarly, Phillips and Rintoul (2000) showed that time periods between 40 h and 90 days, representing mesoscale eddy motions, accounted for roughly 60% of the total eddy flux relative to geographically fixed coordinates, as estimated from current meters located in the Subantarctic Front south of Australia. ALACE av-

erages temperature and velocity measurements separately over part of this frequency band and so cannot precisely represent the high-frequency heat flux. This section uses current meter measurements at time intervals from 1 to 3 h to assess the fraction of the eddy fluxes not sampled by ALACE and to examine the vertical structure of eddy fluxes in the Southern Ocean.

A total of 339 current meter records were examined from 125 locations between 40° and 74°S in the Southern Ocean as shown in Fig. 3. Current meter data were downloaded from the World Ocean Circulation Experiment (WOCE) current meter database (online at kepler.oce.orst.edu/cmdac.html). Details of these moorings as well as heat and momentum flux estimates derived from these moorings have been discussed by a number of authors (e.g., Bryden 1979; Sciremammano et al. 1980; Nowlin et al. 1985; Bryden and Heath 1985; Wunsch 1999; Phillips and Rintoul 2000). Since floats follow the flow like isobaric Lagrangian particles and current meters are Eulerian, their respective eddy statistics may in some cases differ significantly although, if sampling is unbiased, the statistics should be the same.

The earliest of these current meters from the mid-1970s had minimal buoyancy and are known to have

TABLE 3. Summary statistics for heat and momentum fluxes estimated from 339 current meter records from the Southern Ocean. Time-averaged velocities from each current meter have been used to project measurements into along-stream and cross-stream components. These coordinates are fixed in time but differ at each current meter. The velocities u and v refer to the along-stream and cross-stream directions, respectively. Errors about means are equal to one standard deviation divided by the square root of the number of current meter records. Mean fluxes and standard deviations are computed by weighting each current meter record by its record length. To take account of the differing record lengths in the median ratio calculations, first for each current meter record, a mean ratio was determined. A composite data record was then generated in which each current meter record contributed one value of its mean ratio for each day of current meter operation, and the median was determined from this composite dataset. Errors about medians are determined by identifying the range of values making up two-thirds of the observations and (in analogy with standard errors about means) dividing by the square root of the number of current meter records. Within these error bars, simple medians do not differ from the time-weighted medians reported here.

	Heat flux (kW m^{-2})		Momentum flux (cm^2 s^{-2})		
	$\rho C_p \langle u' \theta' \rangle$	$\rho C_p \langle v' \theta' \rangle$	$\langle u'u' \rangle$	$\langle v'v' \rangle$	$\langle u'v' \rangle$
Original	-5.4 ± 1.7	-7.5 ± 1.3	62.3 ± 3.8	52.2 ± 3.6	7.2 ± 3.6
25-day filtered	-0.76 ± 1.3	-5.8 ± 1.0	22.3 ± 2.0	17.8 ± 1.9	3.0 ± 1.5
10-day filtered	-2.9 ± 1.5	-6.9 ± 1.2	33.9 ± 2.6	27.9 ± 2.6	3.3 ± 2.2
Median (25-day/original)	0.61 ± 0.06	0.64 ± 0.06	0.23 ± 0.02	0.25 ± 0.02	0.20 ± 0.02
Median (10-day/original)	0.88 ± 0.07	0.88 ± 0.05	0.44 ± 0.03	0.45 ± 0.02	0.43 ± 0.03

experienced significant mooring motion. Nowlin et al. (1985) carried out a mooring-motion correction and analyzed heat fluxes. They found that mooring motion could increase heat fluxes by as much as 20%. In a comparison of fluxes estimated from corrected and uncorrected Gulf Stream current meter measurements, Wunsch (1999) reported that zonal and meridional heat fluxes in the upper 500 m differed by as much as a factor of 2, but there was no difference in heat fluxes below the upper 500 m. Phillips and Rintoul (2000) updated the mooring-motion methodology developed by Hogg (1991) and Cronin et al. (1992) to compute motion-corrected heat fluxes for the WOCE moorings south of Australia. For current meters 2000 and 3000 m deep on their south mooring, motion-corrected heat fluxes were statistically different from zero (Phillips and Rintoul 2000) and differed from uncorrected fluxes computed for the present study by less than 2%. At shallower depths, nominally 300, 600, and 1000 m, Phillips and Rintoul found that motion-corrected heat fluxes were not statistically different from zero; however, at these depths their corrected fluxes differed from the uncorrected fluxes used for this study both in sign and magnitude.

Of the collected current meter records used here, 144 had pressure measurements. Pressure standard deviations ranged between 0.07 and 256 dbar, with a mean of 50 dbar. Because pressure was available for only a fraction of the moorings, the results shown here have not been corrected for mooring motions. Therefore, even when heat fluxes are statistically significant, actual heat fluxes may differ by 20% or more from the values reported here.

For each current meter that returned velocity and temperature measurements, heat fluxes ($\rho C_p \overline{\mathbf{u}' \theta'}$) were computed in two ways. First the original data (at intervals from 1 to 3 h with tides included) were used to estimate the full heat flux. (Temperatures were converted to potential temperatures assuming salinity to be constant at 34 psu and using measured depth fluctuations

where they were available.) Second, to duplicate the low-frequency filtering of ALACE, velocity and temperature were time-averaged over 10 or 25 days before computing fluxes. Current meter mean velocities were used to project heat fluxes into cross-stream and along-stream components. While some current meter studies have considered heat fluxes relative to time-varying stream coordinates (e.g., Nowlin et al. 1985; Phillips and Rintoul 2000), in order to make comparisons with the ALACE flux estimates, this study looks at heat fluxes only relative to time-averaged stream coordinates determined from the current meters themselves. Repeat deployments at the same location were treated as statistically separate records because of the possibility that the current meter positions shifted slightly with redeployment.

The cross-stream heat fluxes estimated from unfiltered current meter data varied in magnitude from -183 to $+55$ kW m^{-2} and were not normally distributed. The large range of variation was not surprising given the substantial variations in eddy kinetic energy in the Southern Ocean, the differences in depth and dynamical characteristics of the current meter locations, and the large spatial variations in ALACE heat fluxes estimated in the previous section.

To estimate statistical significance of individual heat and eddy flux estimates at each of the current meter locations, the number of degrees of freedom in the time series was first determined by estimating the integral timescale of the current meter records (see, e.g., Nowlin et al. 1985; Wunsch 1999). Both u and v velocities have an average timescale of 10 days, while temperature decorrelates more slowly ($\sim$33 days). In these examples, eddy heat fluxes decorrelate with roughly the same timescale as temperature ($\sim$35 days). Based on this timescale, 51 of the 339 heat fluxes are statistically different from zero at the 90% level. Significant heat fluxes were not strongly concentrated at a single depth, latitude, or longitude in the Southern Ocean.

Table 3 summarizes average eddy heat and momen-

tum fluxes from the 339 current meters, along with 1-standard-deviation error bars, for the original data and for the 10- and 25-day filtered fields. Estimated errors are comparable in magnitude to the means, and means often differ substantially from median values (not shown), indicating the important influence that a few large eddy flux values can have on calculated means. These estimates have been weighted to account for the differing durations of the time series, as discussed in the table caption. These results indicate poleward heat flux on average across the ACC and upstream heat flux along the ACC. Mean heat and momentum fluxes are comparable in magnitude though typically slightly larger than fluxes estimated from ALACE data in section 2. However, the current meter means may not be representative of any clear physical process since they represent a blending of data from different depths, latitudes, and longitudes.

Table 3 indicates that, when averaged over all available current meters, fluxes computed from 25-day and 10-day filtered fields (rows 2 and 3) generally have the same sign as the original fluxes. At each of the current meters, filtered and unfiltered fluxes are also roughly in agreement: Filtered 25-day cross-stream eddy heat fluxes have the same sign as the unfiltered eddy heat fluxes in 78% of the records, and along-stream fluxes agree in sign in 81% of the cases. However, the fluxes from filtered data are generally smaller than the unfiltered fluxes. Rows 4 and 5 of Table 3 show the median ratio of the filtered fluxes to the unfiltered fluxes for 25-day and 10-day averages, respectively. Medians are used rather than means because the flux ratios are nonnormally distributed. Figure 4 shows median ratios for eddy heat and momentum fluxes as a function of averaging time. In Table 3, heat fluxes from 25-day filtered data capture only 60%–65% of the total heat flux, while 10-day ALACE displacements may resolve 85%–90% of the flux. Momentum fluxes filtered over 25 days capture only 20%–25% of the full momentum fluxes, and 10-day filtered momentum fluxes resolve 40%–45% of the momentum fluxes. The fractions of resolved energy estimated here from current meter data are comparable to estimates obtained from Gulf Stream SOFAR float data by Richardson (1992), whose study used a similar approach but did not consider heat fluxes. Thus fluxes computed from ALACE floats are expected to determine the direction of eddy fluxes correctly but to underpredict total heat and momentum fluxes. The next section applies these results in order to correct the ALACE fluxes.

4. Discussion

a. Corrected eddy heat flux

On the basis of the results in section 3, eddy heat and momentum fluxes derived from ALACE in section 2 were readjusted to account for the expected underestimation due to the float sampling. Since the median ratios
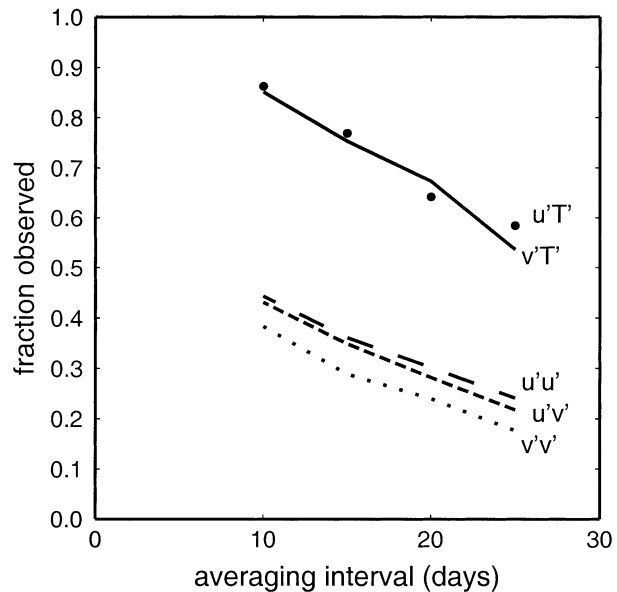

FIG. 4. Median ratios of eddy fluxes computed from time-averaged quantities to total eddy fluxes, shown as a function of averaging time. Ratios are based on results from 339 current meters from locations throughout the Southern Ocean. Resolved eddy flux drops off linearly with increasing averaging time.

of filtered to unfiltered current meter fluxes shown in Fig. 4 decrease linearly with increasing averaging times, linear correction functions were defined for eddy heat and momentum fluxes as a function of ALACE sampling length. Then the eddy fluxes computed from each ALACE displacement were individually rescaled by an appropriate factor, depending on the duration of the displacement. Table 4 reports averages of the resulting revised eddy heat and momentum fluxes for the ACC core. Poleward heat fluxes range between 4.7 ± 2.3 and 7.5 ± 2.9 kW m^{-2} when ALACE provides the mean and are between 8 and $10(\pm 6)$ kW m^{-2} but with larger error bars when the mean is derived from atlas data. These rescaled heat fluxes will be the focus of the remaining discussion.

Table 4 shows that in the ACC core momentum fluxes, like heat fluxes, have along-stream and cross-stream components that are comparable in magnitude. The along-stream component of eddy kinetic energy $\langle u'u' \rangle$ is about 20% larger than the cross-stream component $\langle v'v' \rangle$, while the term $\langle u'v' \rangle$ is significantly smaller than either $\langle u'u' \rangle$ or $\langle v'v' \rangle$. Variance ellipses are often used to assess the orientation and anisotropy of eddy variability (e.g., Morrow et al. 1994). In this analysis, the major and minor axes of variance ellipses are the same within error bars, and the orientation of the variance ellipses relative to the direction of mean flow is not statistically significant. Even if the data are sorted geographically or by dynamic height contour, no statistically significant trend in $\langle u'v' \rangle$ emerges. The results therefore suggest that, within the limitations of the ALACE measurements, mean eddy variability is isotro-

TABLE 4. Eddy heat and momentum fluxes at 900 m in the Southern Ocean, as in Table 2, but scaled to account for underestimation due to 9–25-day averaging. As in Table 2, fluxes represent means in the core of the ACC, as defined by dynamic height limits; and error bars represent the standard error about the mean.

Case	Heat flux (kW m^{-2})		Momentum flux (cm^2 s^{-2})		
	$\rho C_p \langle u' \theta' \rangle$	$\rho C_p \langle v' \theta' \rangle$	$\langle u'u' \rangle$	$\langle v'v' \rangle$	$\langle u'v' \rangle$
	Mean fields from floats				
A	1.2 ± 3.8	-6.2 ± 1.7	153 ± 21	121 ± 17	4.6 ± 3.7
B	1.7 ± 3.3	-4.7 ± 2.3	163 ± 19	125 ± 15	0.3 ± 3.3
C	3.2 ± 3.5	-5.7 ± 2.1	156 ± 21	123 ± 16	2.6 ± 3.0
D	0.4 ± 2.4	-7.3 ± 1.9	138 ± 20	118 ± 17	5.9 ± 3.0
E	0.5 ± 2.4	-7.5 ± 2.9	146 ± 21	113 ± 17	7.4 ± 3.5
F	-1.0 ± 1.9	-7.4 ± 1.7	128 ± 19	113 ± 20	7.0 ± 3.1
G	1.0 ± 3.5	-7.1 ± 1.6	154 ± 21	124 ± 18	4.2 ± 3.1
H	1.8 ± 3.2	-6.1 ± 1.7	149 ± 20	120 ± 16	5.1 ± 2.6
I	0.9 ± 5.6	-5.5 ± 1.9	195 ± 25	126 ± 16	3.1 ± 3.7
J	0.5 ± 2.9	-6.6 ± 1.8	150 ± 21	121 ± 16	4.2 ± 3.0
K	1.0 ± 3.5	-6.7 ± 1.8	155 ± 22	122 ± 17	5.3 ± 3.2
	Mean fields from merged atlas and float				
M	9.4 ± 3.4	-6.8 ± 1.7	164 ± 25	131 ± 23	2.1 ± 28
D_{ref} (m)	Mean fields from atlas				
3000	21 ± 8	-7.7 ± 5.7	181 ± 26	135 ± 20	-3.3 ± 3.9
3500	26 ± 8	-8.8 ± 5.1	177 ± 27	129 ± 19	-3.6 ± 3.7
4000	17 ± 8	-10.1 ± 5.9	180 ± 26	134 ± 19	-2.9 ± 3.8

pic near the core of the ACC, and gradients in $\langle u'v' \rangle$ do not measurably influence the mean flow. This result is not surprising in light of analysis of altimeter data by Hughes and Ash (2001) showing that eddy acceleration and deceleration of the ACC varies on meridional length scales of $O(100 \text{ km})$, which are not well resolved by the available ALACE data.

b. Comparing with other methods: Fluxes in the ACC temperature core

How well do the eddy fluxes in Table 4 agree with results obtained using other methods? Typical estimates of poleward middepth heat flux across the ACC, such as those reported in Table 1, range from -3.7 to -40.6 kW m^{-2}. Reported values vary spatially with lower values occurring on the southern side of the ACC (Nowlin et al. 1985) and with lower estimated fluxes in cases where data are bandpass filtered in time. Altimeter data suggest a similar range of values: Stammer (1998) reported a vertically integrated heat transport in the core of the ACC of $O[-5$ to -15 ($\times 10^6$ W m^{-1})]. If this is assumed to be distributed evenly through the upper 1000 m of the water column, then the expected meridional heat flux in the upper ocean is -5 to -15 kW m^{-2}. These ranges are the same order of magnitude as the cross-stream eddy heat fluxes reported in the second column of Table 4, but the largest estimates from current meters exceed the averages obtained from float data. This is not surprising since the current meter estimates are sensitive to the depths, frequency bands, and coordinate frames used to analyze the data.

Cross-stream eddy heat fluxes from the second column of Table 4 agree within error bars with the mean cross-stream eddy heat flux from current meter data of -7.5 ± 1.3 kW m^{-2} reported in Table 3. However, this comparison may not be meaningful since the current meter data come from a wide range of depths and from regions on the periphery of the ACC, well outside the dynamic height band used for the float analysis. In order to remove the impact of current meters located far from the ACC, mean fluxes were also computed for a subset of current meters with mean temperatures between 2° and 4°C and for float data from the same temperature band. In this case, current-meter-derived eddy heat fluxes exceed float-derived fluxes by a factor of 3. This difference in eddy flux may occur because the current meters deployed in this temperature band have preferentially sampled the upper ocean or the northern part of the ACC, where Drake Passage observations would suggest that we might expect larger poleward eddy heat fluxes (Nowlin et al. 1985).

Along-stream eddy heat transports depend strongly on the method used to calculate them. In the float analysis using the ALACE mean, they are zero within error bars, though typical values are about the same order of magnitude as cross-stream eddy fluxes. In the float analysis using an atlas mean, they are positive, implying downstream heat transport. In contrast, current meter data indicate significant upstream transport of about the same size as the cross-stream eddy heat flux.

These results show that in both current meter and float data, cross-stream eddy heat fluxes are uniformly poleward and statistically significant, while along-stream eddy heat fluxes are comparable in size or smaller than the cross-stream fluxes. Together, these two pieces of evidence imply that at 900-m depth cross-stream eddy

heat flux is not inhibited, and therefore the ACC is not a strong barrier to meridional eddy heat transfer, at least in the isobaric and time-invariant stream coordinate frame used here.

Eddy momentum fluxes from current meter data in Table 3 are of the same order of magnitude as fluxes from ALACE data in Table 4 but are consistently smaller. This is also true when the current data and float data are screened to represent the 2°–4°C temperature band. This difference most likely occurs because eddy momentum fluxes have strongly nonnormal distributions and because current meters cannot survive in the very high eddy energy regions where ALACE floats tend to provide the best sampling. Given the large geographic variations in fluxes and the sparse sampling provided by current meters, the order-of-magnitude agreement is reassuring and more detailed comparison seems unjustifiable.

c. Estimates of vertically integrated heat transport

Translating eddy heat flux at 900-m depth into full water column heat transport requires some knowledge of the vertical structure of the eddy heat fluxes. In the well-studied Gulf Stream region, floats and hydrography suggest that heat and tracers are readily exchanged below the thermocline but that the Gulf Stream acts as a barrier to strong mixing in shallower waters (Owens 1984; Shaw and Rossby 1984; Bower et al. 1985). Park and Gambéroni (1997) found a similar distinction between thermocline waters and deep waters (below about 1000 m) in the region near the Agulhas Return Current where the subtropical and subantarctic fronts nearly merge. However, in most of the Southern Ocean, the ACC differs from the Gulf Stream because it has coherent flow from top to bottom and does not have a well-defined thermocline. Therefore the two distinct mixing regimes found in the Gulf Stream or the Indian Ocean subtropical front cannot be expected to exist in the Circumpolar Current as a whole.

In this study, current meter observations were used to infer a vertical structure for ACC heat flux. Analyses of Drake Passage current meters have sometimes been interpreted to suggest little vertical variation in eddy fluxes (Johnson and Bryden 1989). Sixty-three of the current meters available for this study were from moorings with three or more current meters. As in the Phillips and Rintoul (2000) detailed analysis of current meters south of Australia, these records show that eddy fluxes at a given location decrease with depth, with roughly exponential structures and e-folding depths of $O(1000$ m) (not shown here). Since fluxes drop off sharply with depth, ALACE fluxes at 900-m depth are unlikely to be equivalent to fluxes throughout the entire water column.

Assuming that heat flux decreases with depth with an e-folding scale (H_e) of 1000 m and that the length of the ACC (L) is 23 000 km (corresponding to the circumference of the earth at 55°S), then we can approximate the total vertically integrated heat flux as

$$Q = \oint \int_{-H}^{0} q(z) \, dz \, dx = LH_e \exp(-z_{ref}/H_e)q(z_{ref})$$
$$= 23 \times 10^6 \text{ m} \times 1000 \exp(900/1000)q(900 \text{ m}),$$
$$(1)$$

where H is the ocean depth and z_{ref} is the depth at which heat fluxes q are observed, 900 m in this case. Based on the third column of Table 4, $q(900$ m) is between 4.7 and 7.5 kW m^{-2} for float means implying a vertically integrated flux between $0.27 \pm 0.13 \times 10^{15}$ and $0.42 \pm 0.16 \times 10^{15}$ W. For atlas means, the estimated fluxes between 7.7 and 10.1 kW m^{-2} imply vertically integrated fluxes between 0.4 and $0.6 \pm 0.3 \times 10^{15}$ W. Variations in H_e of ± 400 m change the estimated heat fluxes by less than 10%. These numbers are consistent with previously established ranges for meridional heat flux across the ACC as reported in Table 1 (e.g., de-Szoeke and Levine 1981; Gordon and Owens 1987; Keffer and Holloway 1988).

Poleward eddy heat fluxes have been linked to the surface wind stress that drives the ACC through the mechanism of interfacial form stress. Johnson and Bryden (1989) suggested that heat flux should be proportional to wind stress multiplied by the vertical derivative of potential temperature; that is,

$$\rho_o C_p \overline{v'\theta'} = \frac{C_p \tau^x \overline{\theta_z}}{f}, \quad (2)$$

where τ^x is mean zonal wind stress and is estimated to be about 0.1 N m^{-2} with a variance of 0.15 N m^{-2} (Gille et al. 2001). In GJ atlas data, the vertical derivative of potential temperature, θ_z, at 900-m depth has a mean value for the Southern Ocean of 4×10^{-3} °C m^{-1} but varies geographically: average values along the core of the ACC are 3×10^{-4} °C m^{-1}, an order of magnitude smaller than the regional mean. With this low value of stratification, at 55°S, a minimum poleward heat flux of 1 kW m^{-2} would be required to balance the mean wind stress. The observed heat flux amply exceeds this minimum value.

d. Spatial variation

How do the fluxes estimated from ALACE vary spatially across the ACC? In Fig. 5 mean heat transport ($\rho C_p \langle \overline{v}\overline{\theta} \rangle$) and eddy heat fluxes ($\rho C_p \langle u'\theta' \rangle$ and $\rho C_p \langle v'\theta' \rangle$) have been averaged along dynamic height contours around the entire ACC. Black lines indicate fluxes computed using the case A ALACE mean, and gray lines used the mean derived from GJ atlas data referenced to 3500 m. (The Southern Ocean–wide means of these fluxes are reported as case A in Table 4.) Other cases show qualitatively similar results. Mean along-stream heat transports are uniformly positive and
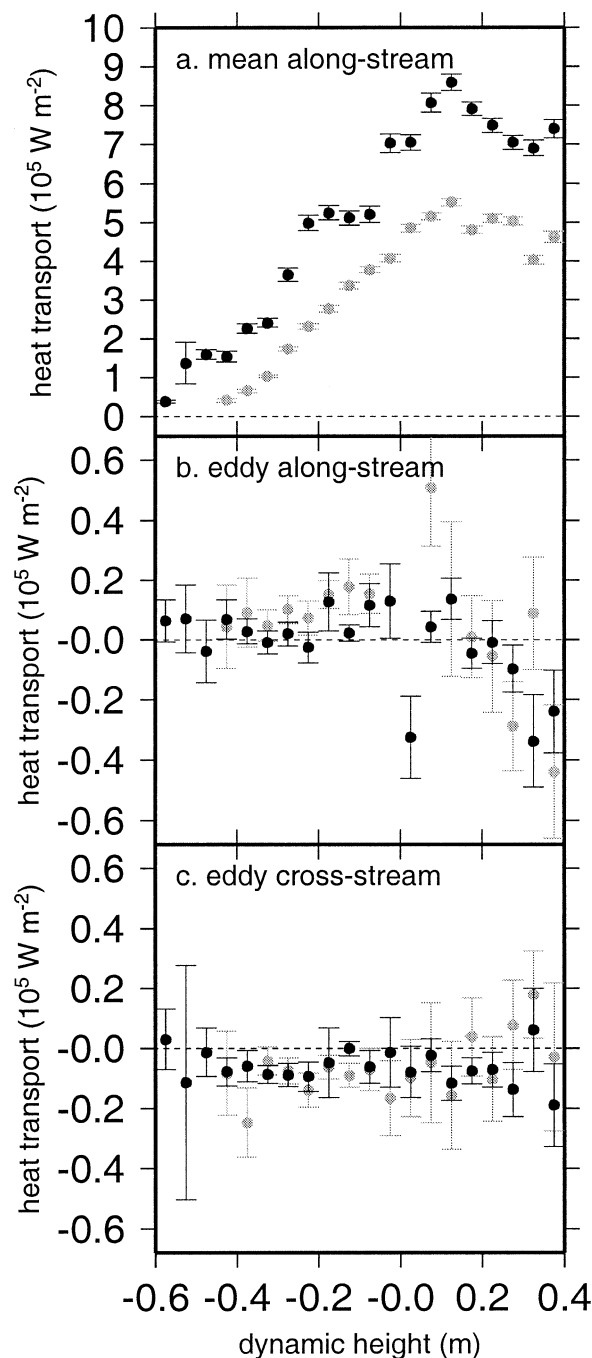
FIG. 5. Rescaled heat transports at 900 m averaged along dynamic height contours, based on mean fields defined by case A in Table 1 of Part I (black) and on mean fields determined from atlas data referenced to 3500 m (gray). (a) Mean along-stream heat transport, (b) along-stream eddy heat transport, and (c) cross-stream eddy heat transport. Dynamic height contours match those shown in Fig. 2 of Part I with 0 corresponding roughly to the center of the ACC and are offset from dynamic heights calculated from bathymetry by 1.05 m. Error bars indicate 1-standard-deviation variations about the mean.

are largest in the core of the subantarctic front, on the north side of the ACC (but, as mentioned earlier, are dependent on the somewhat arbitrary definition of 0°C). Along-stream eddy heat transports are both positive and negative with no consistent sign and no discernible trend as a function of dynamic height. Cross-stream eddy heat fluxes are about the same order of magnitude as along-stream fluxes but are consistently poleward with values of about 5 kW m^{-2} throughout the core of the ACC. Error bars are too large to infer a trend in poleward heat flux as a function of dynamic height contour.

Figure 6 shows bin-averaged cross-stream heat fluxes. In Figs. 6a and 6b, heat fluxes are averaged in 5° latitude by 30° longitude boxes. Figures 6c and 6d show heat fluxes averaged in stream-following boxes delineated by 30° longitude and 0.2 dynamic meter increments. To avoid confusion in places where the mean flow reverses direction, cross-stream fluxes are analyzed only in regions of mean eastward flow.

In Fig. 6, spatial variations in heat fluxes indicate strong poleward eddy heat flux in the western Indian Ocean north of 35°S. The poleward Indian Ocean flux estimates are consistent with basin-scale patterns reported from hydrographic data analyses (Georgi and Toole 1982; Macdonald and Wunsch 1996; Sloyan and Rintoul 2001), suggesting that a major pathway for heat to enter the ACC may exist in the high-eddy region downstream of the Agulhas Retroflection. Moderate poleward heat fluxes occur along the core of the ACC, centered along the 0-m height contour (as shown in Figs. 2c and 2d in Part I). This suggests that heat is transferred poleward along the entire length of the ACC. The color scheme in Fig. 6 suppresses some of the variability in poleward eddy heat fluxes. For example, in Fig. 6d, statistically significant eddy heat flux estimates in the 0 to −0.25 (×10^5 W m^{-2}) band vary between −0.039 × 10^5 and −0.24 (×10^5 W m^{-2}). Elevated fluxes in the core of the ACC are further evidence that the sloping isopycnals of the ACC are not a strong barrier to meridional eddy heat flux. In some cases equatorward heat fluxes occur near Kerguelen Island (70°E), but these fluxes appear to depend on the choice of mean dynamic height and mean temperature. There is no evidence of large equatorward heat flux anywhere in the calculations that use means computed from float data (cases A–I) and average along streamlines (as in Fig. 6d). In contrast, the poleward heat fluxes associated with the Agulhas Retroflection and along the core of the ACC are robust features in all flux maps.

e. Parameterizing eddy heat flux

Eddy heat fluxes are often parameterized in terms of large-scale temperature gradients so that $\langle v'\theta' \rangle \propto \langle \overline{T}_y \rangle$ (Keffer and Holloway 1988; Stammer 1998). Figure 7a shows uncorrected and corrected $\rho C_p \langle v'\theta' \rangle$ as a function of $\langle \overline{T}_y \rangle$ for 0.2 dynamic meter by 30° longitude bin averages computed from case D. The binning used here
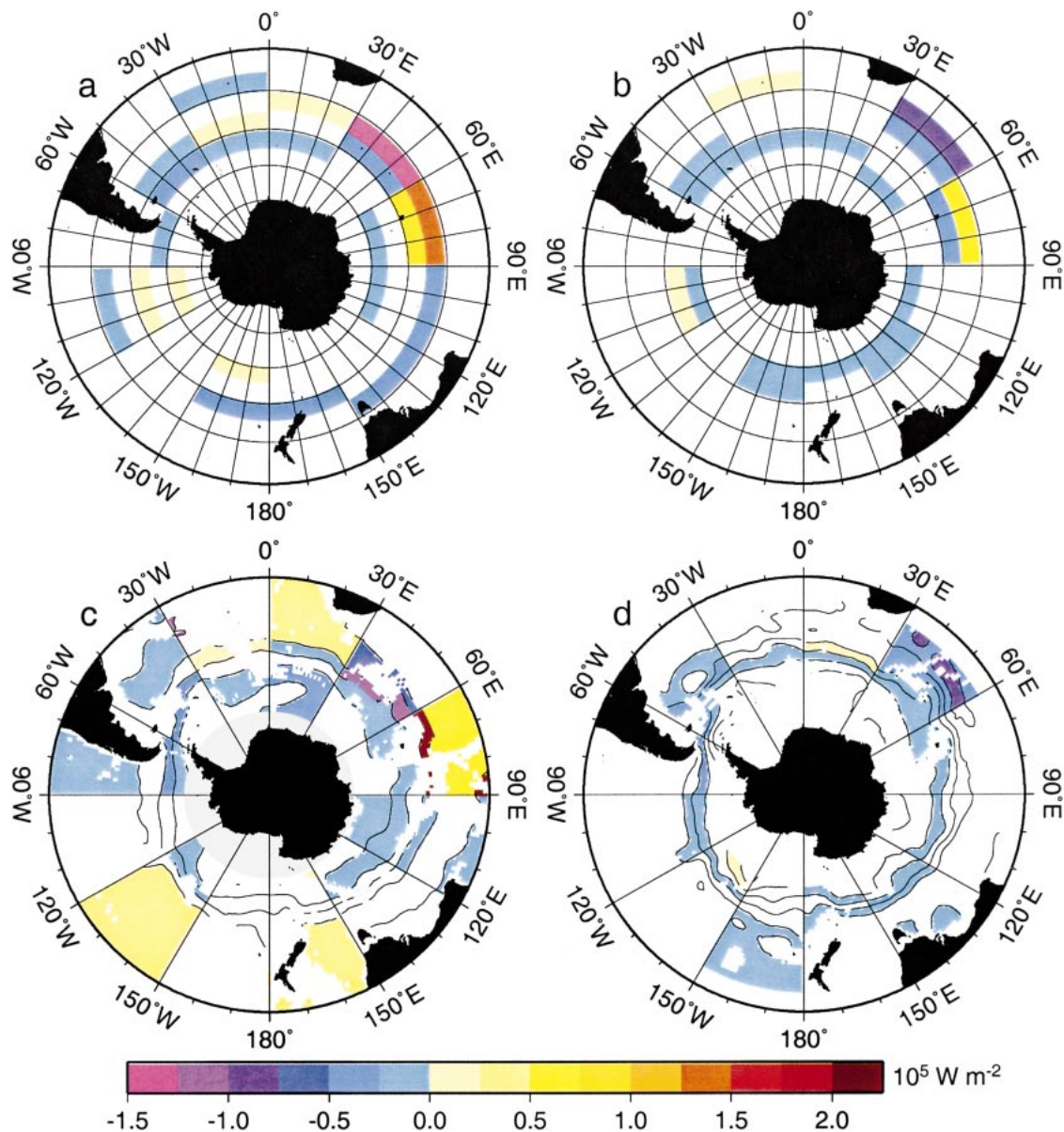
FIG. 6. Cross-ACC (rescaled) eddy heat flux, averaged in (a), (b) 5° lat by 30° lon bins and (c), (d) along streamlines in 0.2 dynamic meter by 30° lon bins. Panels (a) and (c) use means derived from atlas data, and panels (b) and (d) use means from ALACE. Only regions with eastward mean flow are considered, and bins that are not statistically different from zero are not colored. All panels (and other cases not shown) are consistent in showing poleward heat fluxes (negative) occur in the Agulhas Retroflection region and along the core of the ACC. Equatorward heat fluxes primarily occur near Kerguelen Island (70°E), particularly in (a) and (c), which are based on an atlas mean. Contour lines in (c) and (d) delineate the 30° longitude by 0.2 dynamic meter regions used; breaks in contours occur when dynamic height values are not available, usually because the ocean is shallower than 3500 m.

is equivalent to what is shown in Fig. 6d. Case D (with decorrelation scales of 440 km in the zonal direction and 220 km in the meridional direction) was selected for this plot, because it has statistically significant correlation coefficients linking eddy heat fluxes with their possible parameterizations. In this case, the correlation coefficient between uncorrected $\langle v'\theta' \rangle$ and $\langle \overline{T}_y \rangle$ is -0.35, which is statistically significant at the 95% level.

Cases F, J, and K also have statistically significant correlation coefficients between -0.33 and -0.38, while the other cases are not significant. Thus simple parameterizations that assume eddies transfer heat downgradient in proportion to the strength of the large-scale temperature gradient appear likely to account for as much as 40% of the spatial variations in eddy heat flux, though in some situations there may be no statistical
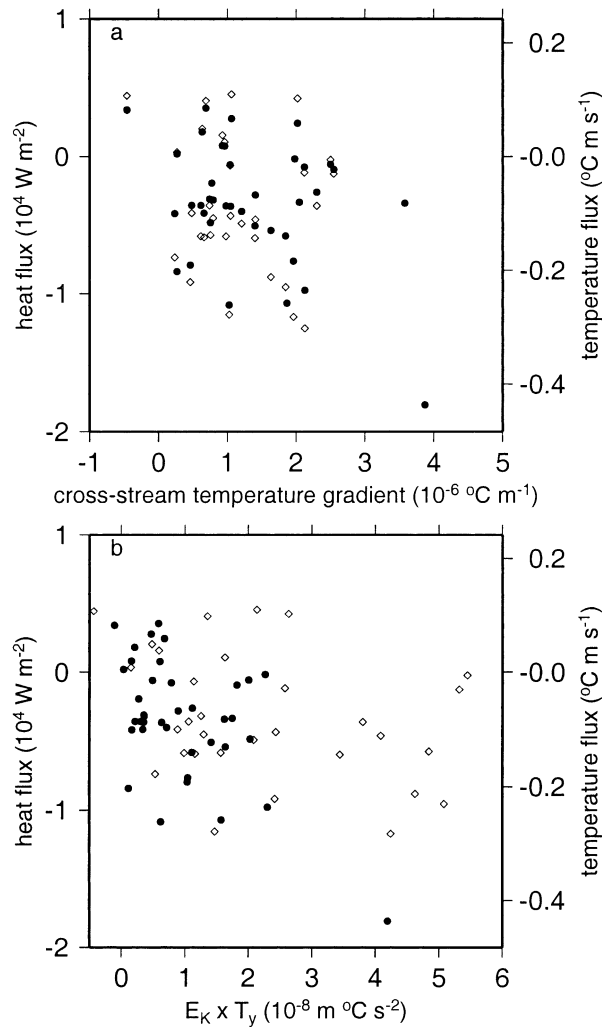
FIG. 7. (a) Eddy heat flux $\rho C_p \langle v' \theta' \rangle$ as a function of $\langle \overline{T}_y \rangle$ for case D. Solid dots show raw heat fluxes; open diamonds are fluxes corrected for the duration of the subsurface displacements. (b) Eddy heat flux as a function of $\langle E_K \rangle \langle \overline{T}_y \rangle$, as in (a). In both cases, only fluxes with error bars less than 10^4 W m^{-2} are shown, although all data were used for least squares fitting.

relationship between heat flux and large-scale temperature gradient. Values of $\langle v' \theta' \rangle$ that have been corrected to account for the duration of ALACE trajectories are not significantly correlated with large-scale temperature gradients, possibly because the statistical correction introduces noise. Along-stream eddy heat fluxes are also not correlated with along-stream temperature gradients at a statistically significant level and will not be discussed.

Least squares fitting a straight line to the uncorrected case-D fluxes (solid circles in Fig. 7) produces $\langle v' \theta' \rangle$ = $(0.0 \pm 0.2) \times 10^{-3}$ m °C s^{-1} $-$ 422 ± 130 m^2 s^{-1} $\langle \overline{T}_y \rangle$ (where heat fluxes have been expressed as temperature fluxes to facilitate comparison with results published elsewhere). The other statistically significant uncorrected fluxes (cases F, J, and K) are the same within

error bars, and the cases that are not statistically significant also agree with these values. Because the correlation coefficients for "corrected" fluxes are not statistically significant, those fits are not reported here, but correction factors are expected to increase the regression coefficient from about 400 to 600 m^2 s^{-1}. These fluxes are comparable to results derived by Stammer (1998) from TOPEX/Poseidon altimeter data; he showed eddy mixing coefficients within the ACC that ranged from about 250 to 1000 m^2 s^{-1}.

In more detailed eddy flux parameterizations, eddy heat transfer also depends on the strength of the local eddy kinetic energy. For example, Stammer (1998) assumed $\langle v' \theta' \rangle \propto \langle E_K \rangle \langle \overline{T}_y \rangle$, where $E_K = u' u' + v' v'$. Figure 7b shows a scatterplot of uncorrected and corrected $\langle v' \theta' \rangle$ as a function of $\langle E_K \rangle \langle \overline{T}_y \rangle$. In this study, for case D the correlation coefficient between $\langle v' \theta' \rangle$ and $\langle E_K \rangle \langle \overline{T}_y \rangle$ is -0.54 for uncorrected fluxes and -0.43 for corrected fluxes. Given the scatter in the data, this diffusion parameterization appears unlikely to be easily tuned in order to explain 100% of the observed heat flux. These correlation coefficients are statistically significant at the 95% level for case D, and overall for 8 of 11 uncorrected cases (cases B–F, H, J, and K) and 4 of 11 corrected cases (cases C, D, H, and J). The fact that correlation coefficients are greater when E_K is included in the regression suggests that eddy kinetic energy has a significant impact on the rate of eddy heat transfer in the ocean.

Case D uncorrected fluxes can be described by a linear least squares fit: $\langle v' \theta' \rangle = 0.8(\pm 1.1)$ ($\times 10^{-4}$ m °C s^{-1}) $-$ $6.3(\pm 1.4) \times 10^4$ s $\langle E_K \rangle \langle \overline{T}_y \rangle$, and corrected fluxes fit: $\langle v' \theta' \rangle = -0.8(\pm 1.7) \times 10^{-4}$ m °C s^{-1} $-$ $2.8(\pm 0.6) \times 10^4$ s $\langle E_K \rangle \langle \overline{T}_y \rangle$. Other cases produce the same results within error bars. These results are consistent with estimates obtained by Stammer (1998), who suggested that the coefficient in front of $E_K \overline{T}_y$ should be $2\alpha\tau \approx 4 \times 10^4$ s, where α, a measure of eddy mixing efficiency, is approximately 0.05, and the timescale $\tau \approx 5$ days in the Southern Ocean.

5. Summary

This study has focused on the eddy heat and momentum fluxes of the Circumpolar Current as inferred from ALACE float observations. ALACE measurements were used to represent instantaneous values of T and $\mathbf{u}$, and time-averaged $\overline{T}$ and $\overline{\mathbf{u}}$ were estimated from objectively mapped fields derived from floats, hydrography, or both. The ALACE data provide the first-ever estimate of cross-ACC eddy fluxes based on subsurface float observations. Results at 900-m depth indicate a poleward eddy heat flux across the ACC between 3.2 and 6.7 kW m^{-2}, with a typical value of 5 kW m^{-2}. Analysis of current meter data suggests that ALACE's temporal smoothing may underestimate the heat flux. After rescaling the eddy heat and momentum fluxes to account for this underestimate and focusing exclusively on the

ACC itself, the resulting fluxes ranged from 5 to 10 kW m^{-2}. Assuming a vertical *e*-folding scale of 1000 m, this implied a total meridional eddy heat flux across the ACC of $0.3(\pm0.1$ to 0.6 $(\pm0.3) \times 10^{15}$ W. In the ACC, cross-stream heat fluxes are larger than or the same order of magnitude as alongstream heat fluxes, suggesting that although the circumpolar path of the ACC prevents the mean flow from carrying a poleward heat transport, isobaric eddy transport does not appear to be inhibited by the sloping isopycnals of the current. The results obtained here are consistent with previous estimates obtained from current meters, suggesting that cross-ACC eddy heat fluxes are not strongly spatially inhomogeneous.

Eddy heat fluxes are statistically correlated both with large-scale temperature gradients alone and with large-scale temperature gradients multiplied by eddy kinetic energy, both of which are commonly used to parameterize heat flux. Least squares fits of regionally averaged eddy heat fluxes to regionally averaged temperature gradients suggest that the large-scale temperature gradient is able to explain about 35% of the eddy heat flux, with an eddy diffusivity of about 400 ± 100 m^2 s^{-1}. The product of eddy kinetic energy and large-scale temperature gradient offers a slightly better parameterization that is able to explain as much as 54% of the eddy heat flux.

Eddy momentum fluxes estimated from ALACE data and from current meter data are nearly isotropic and indicate no measurable cross-stream gradient in momentum flux, implying that within measurement limits, eddies neither accelerate nor decelerate the mean flow. The low horizontal momentum fluxes support the results of numerical modeling studies that have indicated that wind-forced momentum is removed from the ACC via bottom stress rather than through horizontal advection away from the current.

Geographic variations in eddy heat fluxes are substantial. Regardless of the method used to determine mean temperature and velocity, the strongest poleward eddy heat fluxes are seen near the Agulhas Retroflection where Indian Ocean water comes in close contact with the subantarctic front of the ACC. The evidence presented here suggests that heat fluxes are poleward in the fast-moving jets of the ACC, while both poleward and equatorward fluxes are found elsewhere in the Southern Ocean. Together these results imply that heat may enter the ACC in the Indian Ocean sector but that heat travels poleward across the core of the ACC along the entire length of the current.

REFERENCES

Bower, A. S., 1991: A simple kinematic mechanism for mixing fluid parcels across a meandering jet. *J. Phys. Oceanogr.,* **21,** 173–180.

——, H. T. Rossby, and J. L. Lillibridge, 1985: The Gulf Stream—Barrier or blender? *J. Phys. Oceanogr.,* **15,** 24–32.

Bryden, H. L., 1979: Poleward heat flux and conversion of available potential energy in Drake Passage. *J. Mar. Res.,* **37,** 1–22.

——, and R. A. Heath, 1985: Energetic eddies at the northern edge of the Antarctic Circumpolar Current in the southwest Pacific. *Progress in Oceanography,* Vol. 14, Pergamon, 65–87.

——, and S. Imawaki, 2001: Ocean heat transport. *Ocean Circulation and Climate,* G. Siedler et al., Eds., Academic Press, 455–474.

Cronin, M., K. Tracey, and D. R. Watts, 1992: Mooring motion correction of SYNOP central array current meter data. GSO Tech. Rep. No. 92-4, Graduate School of Oceanography, University of Rhode Island, Narragansett, RI, 115 pp.

deSzoeke, R. A., and M. D. Levine, 1981: The advective flux of heat by mean geostrophic motions in the Southern Ocean. *Deep-Sea Res.,* **28,** 1057–1085.

Fukumori, I., R. Raghunath, and L. L. Fu, 1998: Nature of global large-scale sea level variability in relation to atmospheric forcing: A modeling study. *J. Geophys. Res.,* **103,** 5493–5512.

Ganachaud, A., and C. Wunsch, 2000: Improved estimates of global ocean circulation, heat transport and mixing from hydrographic data. *Nature,* **408,** 453–457.

Georgi, D. T., and J. M. Toole, 1982: The Antarctic Circumpolar Current and the oceanic heat and freshwater budgets. *J. Mar. Res.,* **40S,** 183–197.

Gille, S. T., 1999: Mass, heat, and salt transport in the Southeastern Pacific: A Circumpolar Current inverse model. *J. Geophys. Res.,* **104,** 5191–5210.

——, 2003: Float observations of the Southern Ocean. Part I: Estimating mean fields, bottom velocities, and topographic steering. *J. Phys. Oceanogr.,* **33,** 1167–1182.

——, and C. W. Hughes, 2001: Aliasing of high-frequency variability by altimetry: Evaluation from bottom pressure recorders. *Geophys. Res. Lett.,* **28,** 1958–1961.

——, and L. Romero, 2003: Statistical behavior of ALACE floats at the surface of the Southern Ocean. *J. Atmos. Oceanic Technol.,* in press.

——, D. P. Stevens, R. T. Tokmakian, and K. J. Heywood, 2001: Antarctic Circumpolar Current response to zonally-averaged winds. *J. Geophys. Res.,* **106,** 2743–2759.

Gordon, A. L., and W. B. Owens, 1987: Polar oceans. *Rev. Geophys.,* **25,** 227–233.

Gouretski, V. V., and K. Jancke, 1998: A new climatology for the world ocean. WHP SAC Tech. Rep. No. 3, WOCE Rep. 162/98, WOCE Special Analysis Centre, Max-Planck Institute, Hamburg, Germany.

Hogg, N. G., 1991: Mooring motion corrections revisited. *J. Atmos. Oceanic Technol.,* **8,** 289–295.

Hughes, C. W., and E. R. Ash, 2001: Eddy forcing of the mean flow in the Southern Ocean. *J. Geophys. Res.,* **106,** 2713–2722.

Johnson, G. C., and H. L. Bryden, 1989: On the size of the Antarctic Circumpolar Current. *Deep-Sea Res.,* **36,** 39–53.

Keffer, T., and G. Holloway, 1988: Estimating Southern Ocean eddy flux of heat and salt from satellite altimetry. *Nature,* **332,** 624–626.

Keith, D. W., 1995: Meridional energy transport: Uncertainty in zonal means. *Tellus,* **47A,** 30–44.

Lozier, M. S., T. J. Bold, and A. S. Bower, 1996: The influence of propagating waves on cross-stream excursions. *J. Phys. Oceanogr.,* **26,** 1915–1923.

Macdonald, A. M., and C. Wunsch, 1996: An estimate of global ocean circulation and heat fluxes. *Nature,* **382,** 436–439.

Morrow, R., R. Coleman, J. Church, and D. Chelton, 1994: Surface eddy momentum flux and velocity variances in the Southern Ocean from Geosat altimetry. *J. Phys. Oceanogr.,* **24,** 2050–2071.

Nowlin, W. D., Jr., S. J. Worley, and T. Whitworth III, 1985: Methods for making point estimates of eddy heat flux as applied to the Antarctic Circumpolar Current. *J. Geophys. Res.,* **90,** 3305–3324.

Owens, W. B., 1984: A synoptic and statistical description of the Gulf Stream and subtropical gyre using SOFAR floats. *J. Phys. Oceanogr.,* **14,** 104–113.

Park, Y.-H., and L. Gambéroni, 1997: Cross-frontal exchange of Antarctic Intermediate Water and Antarctic Bottom Water in the crozet basin. *Deep-Sea Res.,* **44B,** 963–986.

Phillips, H. E., and S. R. Rintoul, 2000: Eddy variability and energetics from direct current measurements in the Antarctic Circumpolar Current south of Australia. *J. Phys. Oceanogr.,* **30,** 3050–3076.

Richardson, P. L., 1992: Velocity and eddy kinetic energy of the Gulf Stream system from 700-m SOFAR floats subsampled to simulate pop-up floats. *J. Atmos. Oceanic Technol.,* **9,** 495–503.

Sciremammano, F., Jr., R. D. Pillsbury, W. D. Nowlin Jr., and T. Whitworth III, 1980: Spatial scales of temperature and flow in Drake Passage. *J. Geophys. Res.,* **85,** 4015–4028.

Shaw, P. T., and H. T. Rossby, 1984: Towards a Lagrangian description of the Gulf Stream. *J. Phys. Oceanogr.,* **14,** 528–540.

Sloyan, B. M., and S. R. Rintoul, 2000: Estimates of area-averaged diapycnal fluxes from basin-scale budgets. *J. Phys. Oceanogr.,* **30,** 2320–2341.

——, and ——, 2001: The Southern Ocean limb of the global deep overturning circulation. *J. Phys. Oceanogr.,* **31,** 143–173.

Stammer, D., 1998: On eddy characteristics, eddy transports, and mean flow properties. *J. Phys. Oceanogr.,* **28,** 727–739.

Wunsch, C., 1999: Where do ocean eddy heat fluxes matter? *J. Geophys. Res.,* **104,** 13 235–13 249.